



UKAEA-CCFE-PR(25)377

Jan Fikar, Robin Schäublin, Daniel R. Mason, Duc Nguyen-Manh

Mobility of nano-sized 1 2 1 1 1 vacancy and interstitial prismatic dislocation loops in tungsten

Enquiries about copyright and reproduction should in the first instance be addressed to the UKAEA Publications Officer, Culham Science Centre, Building K1/0/83 Abingdon, Oxfordshire, OX14 3DB, UK. The United Kingdom Atomic Energy Authority is the copyright holder.
The contents of this document and all other UKAEA Preprints, Reports and Conference Papers are available to view online free at scientific-publications.ukaea.uk/

Mobility of nano-sized 1 2 1 1 1 vacancy and interstitial prismatic dislocation loops in tungsten

Jan Fikar, Robin Schäublin, Daniel R. Mason, Duc Nguyen-Manh

Mobility of nano-sized ½(1 1 1) vacancy and interstitial prismatic dislocation loops in tungsten

Jan Fikar^{a,*}, Robin Schäublin^b, Daniel R. Mason^c, Duc Nguyen-Manh^c

^aInstitute of Physics of Materials, The Czech Academy of Sciences, Žižkova 22, 616 00 Brno, Czech Republic ^bLaboratory of Metal Physics and Technology, Department of Materials, ETH Zürich, 8093 Zürich, Switzerland ^cCCFE, Culham Campus, Abingdon, Oxfordshire OX14 3DB, United Kingdom

Abstract

The vacancies and interstitials produced in high-energy collision cascades of irradiated tungsten can form prismatic dislocation loops with Burgers vectors $\frac{1}{2}(111)$ and $\frac{1}{2}0$. The $\frac{1}{2}(111)$ loops are very mobile, and their mobility is essential for the microstructure development of irradiated materials, It is a key parameter for predictive models such as kinetic Monte Carlo. We investigated the mobility of $\frac{1}{2}(111)$ vacancy and interstitial hexagonal loops as a function of their size using the recent embedded-atom method tungsten potential. The phonon drag phenomenon occurs at high temperatures and can be separated during post-processing from the thermally activated motion. The magnitude of the phonon drag at 300 K was evaluated and appeared to be critical for single interstitial atoms, with a nearly ten-fold increase of their diffusion, while dislocation loops are less influenced.

Keywords: prismatic dislocation loop, radiation damage, molecular dynamics, mean square displacement, tungsten, diffusion

1. Introduction

Tungsten is a leading candidate material for plasma-facing components in future fusion reactors, valued for its high melting point and resistance to sputtering. However, under operational conditions, its microstructure will be constantly subjected to high-energy particle irradiation, which generates a variety of lattice defects that can degrade its mechanical properties. Recent experimental [1, 2] and computational [3, 4] studies have have shown that these defects are nanoscale prismatic dislocation loops formed directly within displacement cascades.

In tungsten, transmission electron microscope (TEM) observations [5, 6] reveal that these prismatic loops have Burgers vectors of $\frac{1}{2}\langle 111 \rangle$ and $\langle 100 \rangle$. The $\frac{1}{2}\langle 111 \rangle$ loops are highly mobile, whereas the $\langle 100 \rangle$ loops are mobile only at very high temperatures [7]. In the following, we focus on highly mobile $\frac{1}{2}\langle 111 \rangle$ loops in tungsten.

The parameters of thermally activated mobility of the loops are important in predicting the development of the irradiated materials at larger time scales using kinetic Monte Carlo methods. The parameters are usually obtained by several long isothermal molecular dynamics (MD) simulations, where the position of the loop is recorded as a function of the elapsed time. Then, its trajectory is analyzed, and the mean square displacement (MSD) is calculated, which can be related to the diffusivity D using the Einstein diffusion equation.

$$D = \frac{\left\langle (r - r_0)^2 \right\rangle}{2nt},\tag{1}$$

Email address: fikar@ipm.cz (Jan Fikar)

where n is the dimensionality of the movement and t is time. The diffusivity itself is usually thermally activated and obeys the Arrhenius law.

$$D = D_0 \exp\left(\frac{-E_{mig}}{kT}\right),\tag{2}$$

where E_{mig} is the migration energy and D_0 is the diffusivity at infinite temperature. The parameter D_0 corresponds to the situation where the probability of jumping equals one, so the loop will jump to the new position during every attempt.

$$D_0 = b^2 v, \tag{3}$$

where b is the Burgers vector and v is the attempt frequency, sometimes for point defects approximated by Debye frequency.

MSD and diffusivity D obtained for different temperatures T allow us to fit the Arrhenius Eq. 2 and obtain the two parameters for thermally activated motion E_{mig} and D_0 .

Alternatively, E_{mig} can be determined as the energy barrier height using the nudged elastic band (NEB) method [8]. However, NEB does not provide D_0 .

Two limitations of the MSD method for single interstitial atom (SIA) diffusion in tungsten were discovered recently. First, the diffusivity of an SIA in tungsten above 150 K is linear with temperature and does not follow Arrhenius law. This effect is explained by Swinburne *et al.* as a phonon drag phenomenon [9]. Second, the diffusivity at low temperatures is influenced by quantum zero vibrations, and in tungsten, it already appears below 100 K [10]. MSD cannot be efficiently used, as there is not a large enough temperature window to fit the Arrhenius law.

The low-temperature quantum effects are not a problem for classical MSD calculations. The diffusivity calculated by classical MD at low temperatures can be used to fit the Arrhenius

^{*}Corresponding author

parameters D_0 and E_{mig} . On the contrary, Eq. 2 should not be used to determine the real loop mobility at low temperatures D(T < 100 K).

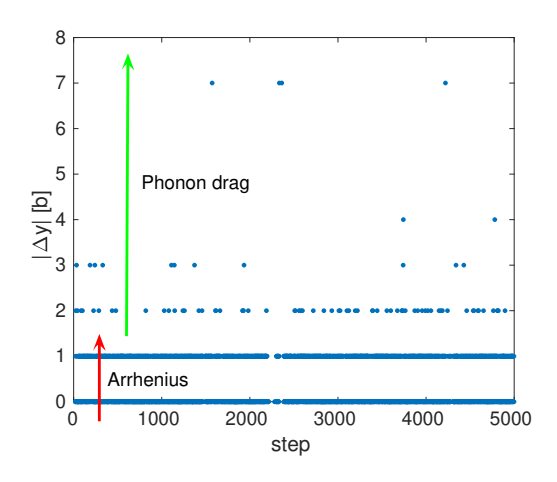
The high-temperature phonon drag is also sometimes explained as a correlation of SIA jumps. In the case of 1D diffusion, the correlation factor f is a ratio of the number of jumps forward and backward relative to the direction of the previous jump. Zhou *et al.* found by MD that the correlation factor for SIA diffusion in tungsten is 2.77-2.44 for temperatures $300-900 \, \mathrm{K}$ [11]. We think that there is no microscopical reason why, in the case of 1D SIA diffusion, the jump should depend on the direction of the previous jump, and thus, in our opinion, f should be equal to 1. We think the observed f > 2 can be explained as jumps longer than one Burgers vector, which are then interpreted as several jumps in the same direction.

We will show how to separate the long jumps by post-processing the MSD data effectively. The objective of this paper is to calculate the parameters of thermally activated diffusivity of the $\frac{1}{2}\langle 1\ 1\ \rangle$ prismatic loops and compare it with diffusivity, including phonon drag phenomenon, also sometimes called correlated diffusion.

2. Computational details

The procedure for creating the sample with the dislocation loops is described in our previous paper [12]. We investigated perfect hexagonal $\frac{1}{2}$ $\langle 1 \ 1 \ 1 \rangle$ loops containing 1, 19, 61, 127, 217, and 397 defects. The hexagonal shape was chosen because it has the lowest formation energy and the highest mobility in tungsten [7]. The largest loop has a diameter of 5.5 nm. Since the dislocation loop creates a long-range deformation field, the simulation block should be at least four times larger than the loop diameter [13]. For the largest loop with 397 defects, the simulation block contains approximately 1.6 million atoms, corresponding to a simulation box side length of 29 nm. The smallest simulation block for single defects and 19-defects loops has 19 thousand atoms and has box side of 7 nm. The nearly cubic simulation boxes with periodic boundary conditions are oriented in directions $\langle \overline{1} 1 0 \rangle$, $\langle 1 1 1 \rangle$, and $\langle 1 1 \overline{2} \rangle$ with the Burgers vector aligned along the y-axis.

The simulation block is first relaxed using the conjugate gradient (CG) method in LAMMPS [14]. It then isothermally evolves for a long time at a specific temperature range of 25 - 800 K. We use the NPT ensemble to accommodate thermal expansion. The long MD simulations tend to accumulate a certain drift due to numerical errors. In our simulations the drift is avoided by periodically zeroing the total momentum of all atoms each 1000 MD steps. Typically, there is a problem detecting the exact loop position at higher temperatures due to the thermal noise. We use molecular dynamics (MD) with an integration time step of Δt of 2 fs and integrate for $1000\Delta t$, i.e. 2 ps, which we call a step. After each step, a restart file is written, from which the simulation can continue seamlessly. Then, a CG is applied to find the precise loop position. The loop is detected using common neighbor analysis (CNA). The average position of the atoms with CNA different from perfect BCC



We will show how to separate the long jumps by post-processing MSD data effectively. The objective of this paper is to calte the parameters of thermally activated diffusivity of the manufacture of the long jumps by post-processing Figure 1: The absolute value of the difference in y position parallel to the Burgers vector of the 127 vacancy loop at 800 K in each step. The jumps up to 1b are considered thermally activated, i.e., Arrhenius, larger jumps represent the phonon drag phenomenon sometimes called the correlated diffusion.

gives the center of the loop. The covariance matrix of the positions of these CNA-detected atoms is also recorded, as its large eigenvalues are a good indication of the loop crossing periodic boundaries. Then, the isothermal MD is continued from the restart file, which results in an uninterrupted simulation. In total we simulate 5000 such steps, corresponding to 10 ns.

A typical result can be seen in Fig. 1, where the absolute value of the difference in position of the loop $|\Delta y|$ in each step is shown. At low temperatures, we observe only jumps up to one Burgers vector *i.e.* 1b, while at higher temperatures around 150–200 K longer jumps start to appear, and their number increases with temperature. The jumps up to 1b are thus considered thermally activated, *i.e.*, Arrhenius behavior, while larger jumps represent the phonon drag phenomenon, also sometimes called correlated diffusion.

Now, we can use all the points, which will give us the total diffusivity, including the phonon drag phenomenon. Alternatively, we can discard all the jumps larger than 1b and calculate thermally activated diffusivity, which can then be used in the Arrhenius fit by Eq. 2. Typically, 10 different temperatures in the 25 – 800 K range are fitted for each loop. Lower temperatures are employed for highly mobile defects, while higher temperatures are used for less mobile defects. It could, in principle, happen that during step two, independent thermally activated jumps occur, which will be during our post-processing incorrectly interpreted as phonon drag. Our chosen step of 2 ps is a compromise, approximately 10 Debye periods long. Shorter steps will decrease the risk of detecting a long jump instead of two short jumps, but it will increase the calculation time, as more CG steps per the same amount of MD steps will be needed.

In our MD simulations, we use the recent embedded atom model (EAM) potential of Mason, Nguyen-Manh, and Becquart (MNB) [15], which is an enhancement of Ackland-Thetford AT potential [16] mainly the in better description of vacancy clusters.

3. Results and discussion

Almost all the loops undergo 1D random motion in the direction of their Burgers vector. There are three exceptions: the single vacancy moves in 3D and with much higher activation energy (see Tab. 3). The SIA exhibits 1D movement up to a temperature of 500 K. Above this temperature, it can change direction, resulting in 3D movement. In this study, we focused solely on the one-dimensional movement of the SIA. The 19 vacancy loop does not move up to 800 K, but at 800 K, its formation energy is gradually decreasing. We conclude that the 19 vacancy loop is at 800 K transforming into a 19 vacancy void, which has lower formation energy, as we discovered in our previous paper [12]. All the vacancy loops up to 50 thousand voids (diameter of 65 nm) will probably transform into energetically favorable voids at sufficiently high temperatures and long times.

The thermal activation parameters as a function of the number of defects N are reported in Fig. 2. The migration energy E_{mig} of the vacancy loops is decreasing with N, while it stays low all the time for interstitial loops. The diffusivity at infinite temperature D_0 seems to be correlated with E_{mig} . For example, lower E_{mig} for 127 interstitial loop is somehow compensated by lower D_0 . This correlation seems to be well fitted by the Meyer-Neldel (MN) enthalpy-entropy compensation rule [17, 18]

$$D_0 = D_{00}e^{E_{mig}/\Delta_{MN}},\tag{4}$$

where D_{00} and Δ_{MN} are constants, the latter is called the MN barrier. The MN rule fit can be seen in Fig. 3; the resulting MN barriers Δ_{MN} are 10 ± 3 meV and 22 ± 3 meV for interstitial and vacancy loops, respectively.

The migration energy of 130 meV for 55 vacancy loop in tungsten was previously reported by Mason *et al.* [5], which agrees well with our values. Becquart *et al.* [19] reported for interstitial loops and SIA in tungsten migration energy of 13 meV and D_0 of $45N^{-1/2}$ Å²/ps. These values are often used in Monte-Carlo simulations. While the migration energy agrees well with our results, our D_0 is about three times smaller for loops and 19 times smaller for SIA. Derlet *et al.* reported a similar migration energy of 39.6 meV and D_0 of 1.19 Å²/ps for 61 vacancy loop in BCC iron [20].

Chen *et al.* reported migration energies and attempt frequencies for SIA and loops consisting of 7-85 interstitials using own Y-C_2 tungsten potential [21]. The values are summarized in Tab. 2. While the D_0 is similar to our values, except for the SIA, the migration energies are higher than our values. It is either caused by difference in the interatomic potentials, or they are higher because the correlated diffusion was not taken into account. Fang *et al.* reported diffusivity at 300 K of 19, 55 and 109 interstitial $\frac{1}{2}\langle 111 \rangle$ loops in Tungsten using the same Y-C_2 tungsten potential [22]. They are 0.52, 0.33 and 0.13 Å²/ps., respectively. Our diffusivity for comparable loops at 300 K are slightly higher. The difference may be explained due to the presence of the free surfaces approximately 12 nm from the loop.

For TEM observations, it is important to know the mobility of loops at RT. The diffusivity at 300 K as predicted by the fitted E_{mig} and D_0 can be seen in Fig. 4. The diffusivity of vacancy

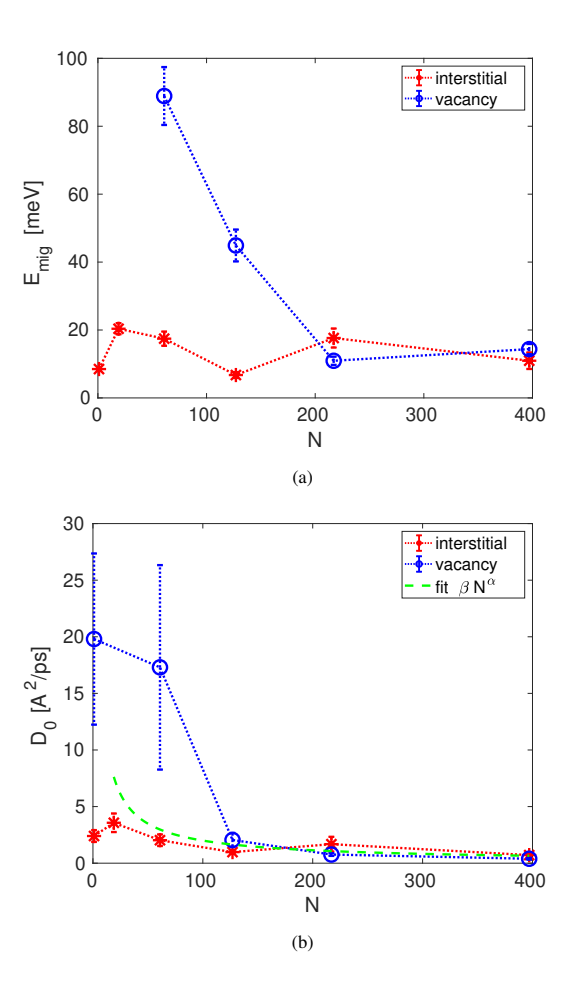


Figure 2: The loop thermally activated mobility parameters obtained by Arrhenius fit as a function of the number of defects N. The error bars correspond to standard deviations. (a) E_{mig} migration energy (note one single vacancy moves in 3D and has an activation energy of $1050 \, \text{meV}$). (b) D_0 diffusivity at infinite temperature. Fitted $\alpha = -0.81 \pm 0.29$, $\beta = 4.4 \pm 1.4 \, \text{Å}^2/\text{ps}$.

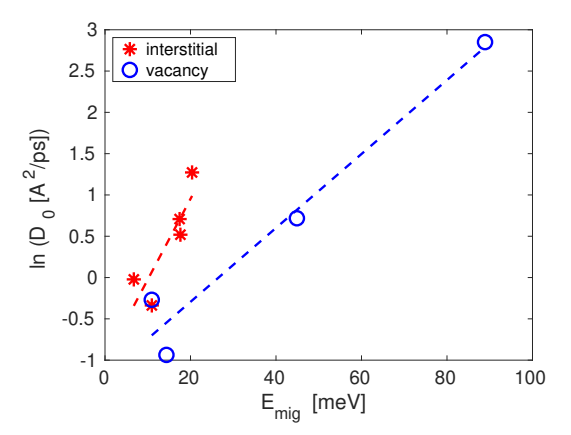


Figure 3: Meyer-Neldel enthalpy-entropy compensation rule for the activation parameters of the loop diffusion. The fitted MN barriers Δ_{MN} are 10 ± 3 meV and 22 ± 3 meV for interstitial and vacancy loops, respectively.

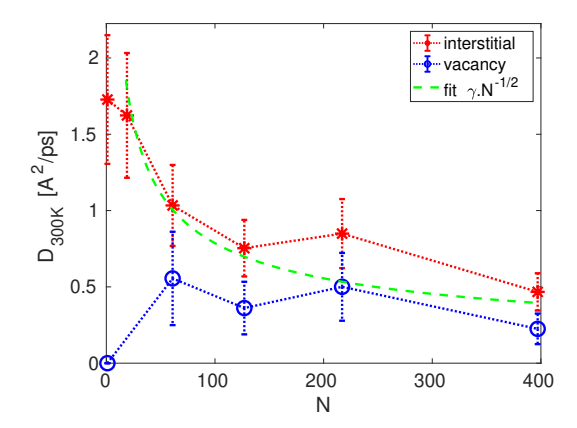


Figure 4: The thermally activated diffusivity of vacancy and interstitial loops at 300 K. The error bars correspond to standard deviations. The interstitial loop diffusivity fitted by $N^{-1/2}$ [20], $\gamma = 7.9 \pm 1.6 \, \text{Å}^2/\text{ps}$.

Table 1: The fitted parameters of thermally activated diffusion for interstitial loops and the predicted thermally activated and total diffusivity at 300 K, including the phonon drag phenomenon. The standard deviations of the fitted E_{mig} , D_0 , and calculated D_{300K} Arrh. are also indicated.

N	E_{mig}	D_0	D_{300K} Arrh.	D_{300K} Total
	[meV]	$[Å^2/ps]$	$[Å^2/ps]$	$[Å^2/ps]$
1	8.50 ± 0.36	2.40 ± 0.52	1.73 ± 0.42	17.52
19	20.37 ± 1.64	3.57 ± 0.82	1.62 ± 0.41	3.56
61	17.45 ± 2.09	2.03 ± 0.51	1.03 ± 0.27	0.86
127	6.74 ± 0.85	0.98 ± 0.10	0.75 ± 0.19	0.82
217	17.64 ± 2.80	1.68 ± 0.65	0.85 ± 0.23	2.59
397	10.95 ± 2.43	0.71 ± 0.22	0.47 ± 0.12	0.38

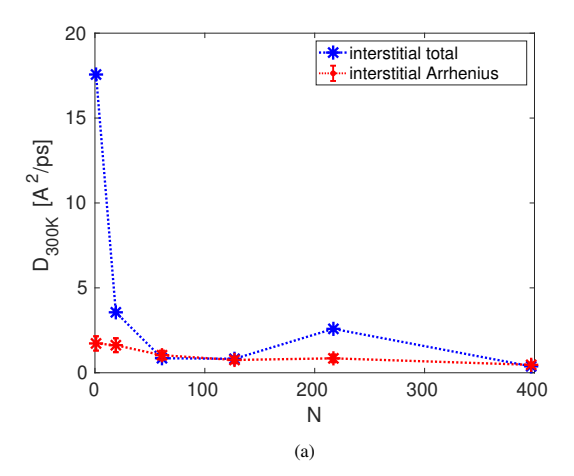
loops is lower than that of interstitial loops, but with increasing N, they are getting closer to each other. The mobility of interstitial loops can be fitted by the $N^{-1/2}$ law proposed for interstitial loops [19, 20]. No such dependency is observed for vacancy loops. A similar experimental dependence of the D_0 prefactor on loop size in iron $N^{-0.8}$ was reported by Arakawa *et al.* [23]. Our prefactor D_0 seems to follow the same $N^{-0.81\pm0.29}$ for interstitial and vacancy loops if the results for a single vacancy and a single interstitial (N = 1) are omitted.

For comparison, we can at 300 K calculate the diffusivity D_{300K} Total, including the phonon drag phenomenon, by not discarding the jumps larger than 1b. A comparison of D_{300K} Arrh. and Total can be seen in Fig. 5. At 300 K the phonon drag phenomenon is significant only for SIA, while the dislocation loops are influenced much less.

The fitted thermally activated parameters E_{mig} and D_0 together with D_{300K} Arrh. and D_{300K} Total are reported in Tabs. 1 and 3. Note that D_{300K} Arrh. are obtained from fitted E_{mig} and D_0 , while D_{300K} Total is a result of a single MSD simulation at 300 K.

4. Conclusions

We have investigated the diffusivity of the hexagonal vacancy and interstitial $\frac{1}{2}(111)$ loops by MSD and developed



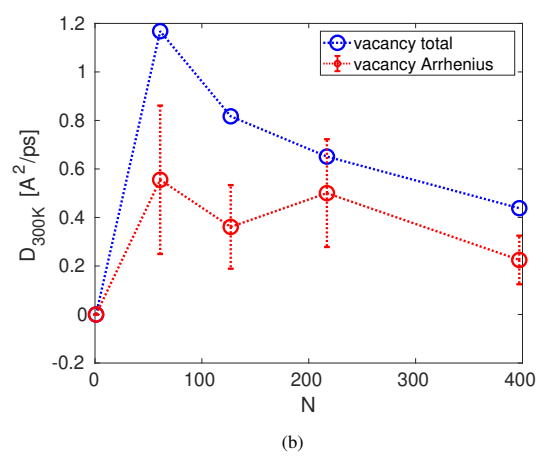


Figure 5: The thermally activated and total mobility, including the phonon drag phenomenon. (a) for interstitial loops and (b) for vacancy loops. The error bars in the thermally activated case correspond to standard deviations.

Table 2: Parameters of thermally activated diffusion for interstitial loops from [21] for comparison.

	N	E_{mig}	D_0
		[meV]	$[Å^2/ps]$
	1	44	10.4
	7	26	4.7
•	19	31	4.0
	37	30	3.2
	61	25	2.2
	85	29	2.0

Table 3: The fitted parameters of thermally activated diffusion for vacancy loops and the predicted thermally activated and total diffusivity at 300 K, including the phonon drag phenomenon. The standard deviations of the fitted E_{mig} , D_0 , and calculated D_{300K} Arrh. are also indicated.

N	E_{mig}	D_0	D_{300K} Arrh.	D_{300K} Total
	[meV]	$[Å^2/ps]$	$[Å^2/ps]$	$[\mathring{A}^2/ps]$
1	1050 ± 60	19.8 ± 7.56	0	0
19	-	-	-	-
61	88.90 ± 8.52	17.3 ± 9.03	0.55 ± 0.31	1.17
127	44.89 ± 4.69	2.05 ± 0.62	0.36 ± 0.17	0.82
217	10.94 ± 1.21	0.76 ± 0.12	0.50 ± 0.22	0.65
397	14.37 ± 1.52	0.39 ± 0.08	0.22 ± 0.10	0.44

a method to eliminate the influence of the phonon drag phenomenon at high temperatures, which is sometimes referred to as correlated diffusion. Our specific conclusions are the following:

- The mobility of small vacancy loops is lower than that of the corresponding interstitial loops. At larger sizes, the mobility becomes comparable, and perfect dislocation loops "forget" their point defect nature.
- The migration barrier decreases with size for vacancy loops, while it remains low and almost constant for interstitial loops.
- The diffusivity of interstitial loops follows the $N^{-1/2}$ law; this is not true for vacancy loops.
- At RT, the phonon drag phenomenon increases the SIA diffusion by nearly 10 times, while the vacancy and interstitial loops diffusion is less affected.
- At higher temperatures, the phonon drag must be considered for both SIA and dislocation loop diffusion. In general, phonon drag should be accounted for in all high-temperature diffusion scenarios with low migration barriers.
- The 19 vacancy ½(1 1 1) loop does not move; instead, it transforms at 800 K to energetically more favorable 19 vacancy void. A similar transformation likely occurs at high temperatures for all vacancy loops with diameters below 65 nm.
- Our method enables the accurate calculation of thermal activation parameters from correlated diffusion by effectively subtracting the phonon drag phenomenon.

Acknowledgments

Computational resources were provided by the e-INFRA CZ project (ID:90254), supported by the Ministry of Education, Youth and Sports of the Czech Republic. This work has been carried out within the framework of the EUROfusion Consortium, funded by the European Union via the Euratom Research and Training Programme (Grant Agreement No 101052200 — EUROfusion) and from the EPSRC [grant number EP/W006839/1]. Views and opinions expressed are, however, those of the author(s) only and do not necessarily reflect those of the European Union or the European Commission. Neither the European Union nor the European Commission can be held responsible for them.

References

- X. Yi, A. E. Sand, D. R. Mason, M. A. Kirk, S. G. Roberts, K. Nordlund, S. L. Dudarev, EPL 110 (3) (2015) 36001.
- [2] D. R. Mason, A. E. Sand, X. Yi, S. L. Dudarev, Acta Mater. 144 (2017) 905–917.
- [3] A. E. Sand, S. L. Dudarev, K. Nordlund, EPL 103 (4) (2013) 46003.

- [4] A. E. Sand, D. R. Mason, A. D. Backer, X. Yi, S. L. Dudarev, K. Nord-lund, Materials Research Letters 5 (5) (2017) 357–363.
- [5] D. R. Mason, X. Yi, M. A. Kirk, S. L. Dudarev, J. Phys.-Condens. Mat. 26 (37) (2014) 375701.
- [6] F. Ferroni, X. Yi, K. Arakawa, S. P. Fitzgerald, P. D. Edmondson, S. G. Roberts, Acta Mater. 90 (2015) 380–393.
- [7] J. Fikar, R. Gröger, R. Schäublin, Nucl. Instrum. Meth. B 393 (2017) 186 – 189
- [8] H. Jónsson, G. Mills, K. W. Jacobsen, Classical and Quantum Dynamics in Condensed Phase Simulations, World Scientific, 1998.
- [9] T. D. Swinburne, S. L. Dudarev, Phys. Rev. B 92 (2015) 134302.
- [10] T. D. Swinburne, P.-W. Ma, S. L. Dudarev, New J. Phys. 19 (2017) 073024.
- [11] W. Zhou, Y. Li, L. Huang, Z. Zeng, X. Ju, J. of Nucl. Mater. 437 (2013) 438 – 444.
- [12] J. Fikar, R. Schäublin, D. R. Mason, D. Nguyen-Manh, Nucl. Mater. Energy 16 (2018) 60–65.
- [13] J. Fikar, R. Schäublin, Nucl. Instrum. Meth. B 267 (2009) 3218–3222.
- [14] S. Plimpton, J. Comp. Phys. 117 (1995) 1-19.
- [15] D. R. Mason, D. Nguyen-Manh, C. S. Becquart, J. Phys.: Condens. Mat. 29 (2017) 505501.
- [16] G. J. Ackland, R. Thetford, Philos. Mag. A 56 (1987) 15-30.
- [17] W. Meyer, H. Neldel, Z. Tech. Phys. 12 (1937) 588.
- [18] A. Yelon, B. Movaghar, H. M. Branz, Phys. Rev. B 46 (1992) 12244– 12250.
- [19] C. Becquart, C. Domain, U. Sarkar, A. DeBacker, M. Hou, Journal of Nuclear Materials 403 (1) (2010) 75–88.
- [20] P. M. Derlet, M. R. Gilbert, S. L. Dudarev, Phys. Rev. B 84 (2011) 134109.
- [21] Y. Chen, J. Fang, L. Liu, W. Hu, C. Jiang, N. Gao, H.-B. Zhou, G.-H. Lu, F. Gao, H. Deng, Journal of Nuclear Materials 522 (2019) 200–211.
- [22] J. Fang, L. Liu, N. Gao, W. Hu, F. Gao, H. Deng, Journal of Applied Physics 128 (6) (2020) 065103.
- [23] K. Arakawa, K. Ono, M. Isshiki, K. Mimura, M. Uchikoshi, H. Mori, Science 318 (2007) 956–959.